Structure, nonlinear properties, and photosensitivity of (GeSe2)100-x(Sb2Se3)x glasses

Mélinda Olivier, J.C. Tchahame, Petr Nemec, Mathieu Chauvet, V. Besse, C. Cassagne, G. Boudebs, G. Renversez, Rémi Boidin, Emeline Baudet, et al.

Structure, nonlinear properties, and photosensitivity of $(GeSe_2)_{100-x}(Sb_2Se_3)_x$ glasses

M. Olivier,[1] J.C. Tchahame,[2] P. Němec,[1] M. Chauvet,[2] V. Besse,[3] C. Cassagne,[3] G. Boudebs,[3] G. Renversez,[4] R. Boidin,[1] E. Baudet,[5] and V. Nazabal [5,*]

[1]*Department of Graphic Arts and Photophysics, Faculty of Chemical Technology, University of Pardubice, Studentská 573, 53210 Pardubice, Czech Republic*
[2]*FEMTO-ST, UMR 6174, Université de Franche Comté, 16, route de Gray, 25000 Besançon, France*
[3]*LUNAM Université, Université d'Angers, LPhiA, Laboratoire de Photoniques d'Angers, EA 4464, 2 Boulevard Lavoisier, 49045 Angers Cedex 01, France*
[4]*Institut Fresnel, UMR 7249, Université d'Aix Marseille, Campus de Saint Jérôme, 13013 Marseille, France*
[5]*Institut des sciences chimiques de Rennes, UMR CNRS 6226, Equipe Verres et Céramiques, Université de Rennes 1, 35042 Rennes, France*
virginie.nazabal@univ-rennes1.fr

Abstract: Chalcogenide glasses from $(GeSe_2)_{100-x}(Sb_2Se_3)_x$ system were synthesized, with x varying from 5 to 70, in order to evaluate the influence of antimony selenide addition on nonlinear optical properties and photosensitivity. Nonlinear refractive index and two photon absorption coefficients were measured both at 1064 nm in picosecond regime using the Z-scan technique and at 1.55 µm in femtosecond regime using an original method based on direct analysis of beam profile change while propagating in the chalcogenide glasses. The study of their photosensitivity at 1.55 µm revealed highly glass composition dependent behavior and quasi-photostable compositions have been identified in femtosecond regime. To better understand these characteristics, the evolution of the glass transition temperature, density and structure with the chemical composition were determined.

OCIS codes: (160.2750) Glass and other amorphous materials; (160.4760) Optical properties; (190.4400) Nonlinear optics, materials; (300.6450) Spectroscopy, Raman.

References

1. C. Meneghini and A. Villeneuve, "As_2S_3 photosensitivity by two-photon absorption: holographic gratings and self-written channel waveguides," J. Opt. Soc. Am. B **15**(12), 2946–2950 (1998).
2. K. Shimakawa, A. Kolobov, and S. R. Elliott, "Photoinduced effects and metastability in amorphous semiconductors and insulators," Adv. Phys. **44**(6), 475–588 (1995).
3. N. Hô, J. M. Laniel, R. Vallée, and A. Villeneuve, "Photosensitivity of As_2S_3 chalcogenide thin films at 1.5 microm," Opt. Lett. **28**(12), 965–967 (2003).
4. P. Němec, S. Zhang, V. Nazabal, K. Fedus, G. Boudebs, A. Moreac, M. Cathelinaud, and X.-H. Zhang, "Photo-stability of pulsed laser deposited $Ge_xAs_ySe_{100-x-y}$ amorphous thin films," Opt. Express **18**(22), 22944–22957 (2010).
5. G. Lenz, J. Zimmermann, T. Katsufuji, M. E. Lines, H. Y. Hwang, S. Spälter, R. E. Slusher, S. W. Cheong, J. S. Sanghera, and I. D. Aggarwal, "Large Kerr effect in bulk Se-based chalcogenide glasses," Opt. Lett. **25**(4), 254–256 (2000).
6. C. Quemard, F. Smektala, V. Couderc, A. Barthelemy, and J. Lucas, "Chalcogenide glasses with high non linear optical properties for telecommunications," J. Phys. Chem. Solids **62**(8), 1435–1440 (2001).
7. A. Zakery and S. R. Elliott, "Optical properties and applications of chalcogenide glasses: a review," J. Non-Cryst. Solids **330**(1-3), 1–12 (2003).
8. J. S. Sanghera, C. M. Florea, L. B. Shaw, P. Pureza, V. Q. Nguyen, M. Bashkansky, Z. Dutton, and I. D. Aggarwal, "Non-linear properties of chalcogenide glasses and fibers," J. Non-Cryst. Solids **354**(2-9), 462–467 (2008).
9. S. J. Madden, D. Y. Choi, M. R. E. Lamont, V. G. Ta'eed, N. J. Baker, M. D. Pelusi, B. Luther-Davies, and B. J. Eggleton, "Chalcogenide glass photonic chips," Opt. Photonics News **19**(2), 18–23 (2008).
10. B. J. Eggleton, B. Luther-Davies, and K. Richardson, "Chalcogenide photonics," Nat. Photonics **5**, 141–148 (2011).

#203558 - $15.00 USD Received 23 Dec 2013; revised 18 Feb 2014; accepted 19 Feb 2014; published 25 Feb 2014

11. C. Monat, M. Spurny, C. Grillet, L. O'Faolain, T. F. Krauss, B. J. Eggleton, D. Bulla, S. Madden, and B. Luther-Davies, "Third-harmonic generation in slow-light chalcogenide glass photonic crystal waveguides," Opt. Lett. **36**(15), 2818–2820 (2011).
12. T. D. Vo, R. Pant, M. D. Pelusi, J. Schröder, D. Y. Choi, S. K. Debbarma, S. J. Madden, B. Luther-Davies, and B. J. Eggleton, "Photonic chip-based all-optical XOR gate for 40 and 160 Gbit/s DPSK signals," Opt. Lett. **36**(5), 710–712 (2011).
13. M. D. Pelusi, F. Luan, S. Madden, D. Y. Choi, D. A. Bulla, B. Luther-Davies, and B. J. Eggleton, "Wavelength conversion of high-speed phase and intensity modulated signals using a highly nonlinear chalcogenide glass chip," IEEE Photon. Technol. Lett. **22**(1), 3–5 (2010).
14. M. Sheik-Bahae, D. C. Hutchings, D. J. Hagan, and E. W. Vanstryland, "Dispersion of bound electronic nonlinear refraction in solids," IEEE J. Quantum Electron. **27**(6), 1296–1309 (1991).
15. M. Sheik-Bahae and E. W. Van Stryland, "Optical nonlinearities in the transparency region of bulk semiconductors," in "*Nonlinear Optics in Semiconductors I,*" vol. 58 of Semiconductors and Semimetals, E. Garmire and A. Kost, eds. (Elsevier, 1998), chap. 4, pp. 257–318.
16. S. Kasap and P. Capper, eds., *Springer Handbook of Electronic and Photonic Materials* (Springer, 2006).
17. K. Tanaka, "Nonlinear optics in glasses: How can we analyze?" J. Phys. Chem. Solids **68**(5-6), 896–900 (2007).
18. H. Nasu, K. Kubodera, M. Kobayashi, M. Nakamura, and K. Kamiya, "3rd-harmonic generation from some chalcogenide glasses," J. Am. Ceram. Soc. **73**(6), 1794–1796 (1990).
19. J. M. Harbold, F. O. Ilday, F. W. Wise, and B. G. Aitken, "Highly nonlinear Ge-As-Se and Ge-As-S-Se glasses for all-optical switching," IEEE Photon. Technol. Lett. **14**(6), 822–824 (2002).
20. J. M. Harbold, F. O. Ilday, F. W. Wise, J. S. Sanghera, V. Q. Nguyen, L. B. Shaw, and I. D. Aggarwal, "Highly nonlinear As-S-Se glasses for all-optical switching," Opt. Lett. **27**(2), 119–121 (2002).
21. T. Cardinal, K. A. Richardson, H. Shim, A. Schulte, R. Beatty, K. Le Foulgoc, C. Meneghini, J. F. Viens, and A. Villeneuve, "Non-linear optical properties of chalcogenide glasses in the system As-S-Se," J. Non-Cryst. Solids **257**, 353–360 (1999).
22. G. Lenz and S. Spalter, "Chalcogenide glasses," Nonlinear Photonic Crystals **10**, 255–267 (2003).
23. F. Smektala, C. Quemard, L. Leneindre, J. Lucas, A. Barthelemy, and C. De Angelis, "Chalcogenide glasses with large non-linear refractive indices," J. Non-Cryst. Solids **239**(1-3), 139–142 (1998).
24. S. Cherukulappurath, M. Guignard, C. Marchand, F. Smektala, and G. Boudebs, "Linear and nonlinear optical characterization of tellurium based chalcogenide glasses," Opt. Commun. **242**(1-3), 313–319 (2004).
25. J. T. Gopinath, M. Soljacic, E. P. Ippen, V. N. Fuflyigin, W. A. King, and M. Shurgalin, "Third order nonlinearities in Ge-As-Se-based glasses for telecommunications applications," J. Appl. Phys. **96**(11), 6931–6933 (2004).
26. L. Petit, N. Carlie, H. Chen, S. Gaylord, J. Massera, G. Boudebs, J. Hu, A. Agarwal, L. Kimerling, and K. Richardson, "Compositional dependence of the nonlinear refractive index of new germanium-based chalcogenide glasses," J. Solid State Chem. **182**(10), 2756–2761 (2009).
27. R. Golovchak, O. Shpotyuk, M. Iovu, A. Kovalskiy, and H. Jain, "Topology and chemical order in As(x)Ge(x)Se(1-2x) glasses: A high-resolution X-ray photoelectron spectroscopy study," J. Non-Cryst. Solids **357**(19-20), 3454–3460 (2011).
28. M. A. Popescu, *Non-Crystalline Chalcogenides* (Kluwer Academic Publishers, Dordrecht, 2000).
29. J. Wang, M. Sheik-Bahae, A. A. Said, D. J. Hagan, and E. W. Van Stryland, "Time-resolved Z-scan measurements of optical nonlinearities," J. Opt. Soc. Am. B **11**(6), 1009–1017 (1994).
30. G. Boudebs and K. Fedus, "Absolute measurement of the nonlinear refractive indices of reference materials," J. Appl. Phys. **105**(10), 103106 (2009).
31. G. Lucovsky, A. Mooradian, W. Taylor, G. B. Wright, and R. C. Keezer, "Identification of the fundamental vibrational modes of trigonal, α - monoclinic and amorphous selenium," Solid State Commun. **5**(2), 113–117 (1967).
32. M. Wihl, M. Cardona, and J. Tauc, "Raman scattering in amorphous Ge and III–V compounds," J. Non-Cryst. Solids **8–10**, 172–178 (1972).
33. T. Fukunaga, Y. Tanaka, and K. Murase, "Glass formation and vibrational properties in the (Ge, Sn)-Se system," Solid State Commun. **42**(7), 513–516 (1982).
34. K. Murase, T. Fukunaga, K. Yakushiji, T. Yoshimi, and I. Yunoki, "Investigation of stability of (Ge, Sn)-(S, or Se)$_{4/2}$ cluster vibrational spectra," J. Non-Cryst. Solids **59–60**(Part 2), 883–886 (1983).
35. S. Sugai, "Stochastic random network model in Ge and Si chalcogenide glasses," Phys. Rev. B **35**(3), 1345–1361 (1987).
36. O. Matsuda, K. Inoue, and K. Murase, "Resonant Raman study on crystalline $GeSe_2$ in relation to amorphous states," Solid State Commun. **75**(4), 303–308 (1990).
37. K. Jackson, A. Briley, S. Grossman, D. V. Porezag, and M. R. Pederson, "Raman-active modes of a-$GeSe_2$ and a-GeS_2: A first-principles study," Phys. Rev. B **60**(22), 14985–14989 (1999).
38. L. Petit, N. Carlie, K. Richardson, Y. Guo, A. Schulte, B. Campbell, B. Ferreira, and S. Martin, "Effect of the substitution of S for Se on the structure of the glasses in the system $Ge_{0.23}Sb_{0.07}S_{0.70-x}Se_x$," J. Phys. Chem. Solids **66**(10), 1788–1794 (2005).
39. J. E. Griffiths, G. P. Espinosa, J. C. Phillips, and J. P. Remeika, "Raman spectra and athermal laser annealing of $Ge(S_xSe_{1-x})_2$ glasses," Phys. Rev. B **28**(8), 4444–4453 (1983).

#203558 - $15.00 USD Received 23 Dec 2013; revised 18 Feb 2014; accepted 19 Feb 2014; published 25 Feb 2014

40. V. Nazabal, P. Nemec, A. M. Jurdyc, S. Zhang, F. Charpentier, H. Lhermite, J. Charrier, J. P. Guin, A. Moreac, M. Frumar, and J. L. Adam, "Optical waveguide based on amorphous Er^{3+}-doped Ga–Ge–Sb–S(Se) pulsed laser deposited thin films," Thin Solid Films **518**(17), 4941–4947 (2010).
41. L. Petit, N. Carlie, R. Villeneuve, J. Massera, M. Couzi, A. Humeau, G. Boudebs, and K. Richardson, "Effect of the substitution of S for Se on the structure and non-linear optical properties of the glasses in the system $Ge_{0.18}Ga_{0.05}Sb_{0.07}S_{0.70-x}Se_x$," J. Non-Cryst. Solids **352**(50-51), 5413–5420 (2006).
42. P. Nemec, B. Frumarová, and M. Frumar, "Structure and properties of the pure and Pr^{3+}-doped $Ge_{25}Ga_5Se_{70}$ and $Ge_{30}Ga_5Se_{65}$ glasses," J. Non-Cryst. Solids **270**(1-3), 137–146 (2000).
43. V. Nazabal, F. Charpentier, J.-L. Adam, P. Nemec, H. Lhermite, M.-L. Brandily-Anne, J. Charrier, J.-P. Guin, and A. Moréac, "Sputtering and pulsed laser deposition for near- and mid-infrared applications: A comparative study of $Ge_{25}Sb_{10}S_{65}$ and $Ge_{25}Sb_{10}Se_{65}$ amorphous thin films," Int. J. Appl. Ceram. Technol. **8**(5), 990–1000 (2011).
44. Z. G. Ivanova, E. Cernoskova, V. S. Vassilev, and S. V. Boycheva, "Thermomechanical and structural characterization of $GeSe_2$–Sb_2Se_3–ZnSe glasses," Mater. Lett. **57**(5-6), 1025–1028 (2003).
45. L. Petit, N. Carlie, F. Adamietz, M. Couzi, V. Rodriguez, and K. C. Richardson, "Correlation between physical, optical and structural properties of sulfide glasses in the system Ge–Sb–S," Mater. Chem. Phys. **97**(1), 64–70 (2006).
46. P. Nemec, A. Moreac, V. Nazabal, M. Pavlista, J. Prikryl, and M. Frumar, "Ge-Sb-Te thin films deposited by pulsed laser: An ellipsometry and Raman scattering spectroscopy study," J. Appl. Phys. **106**(10), 103509 (2009).
47. L. Petit, N. Carlie, A. Humeau, G. Boudebs, H. Jain, A. C. Miller, and K. Richardson, "Correlation between the nonlinear refractive index and structure of germanium-based chalcogenide glasses," Mater. Res. Bull. **42**(12), 2107–2116 (2007).
48. J. Troles, F. Smektala, G. Boudebs, and A. Monteil, "Third order nonlinear optical characterization of new chalcohalogenide glasses containing lead iodine," Opt. Mater. **22**(4), 335–343 (2003).
49. D. Milam, "Review and assessment of measured values of the nonlinear refractive-index coefficient of fused silica," Appl. Opt. **37**(3), 546–550 (1998).
50. G. Boudebs, S. Cherukulappurath, H. Leblond, J. Troles, F. Smektala, and F. Sanchez, "Experimental and theoretical study of higher-order nonlinearities in chalcogenide glasses," Opt. Commun. **219**(1-6), 427–433 (2003).
51. A. A. Said, M. Sheik-Bahae, D. J. Hagan, T. H. Wei, J. Wang, J. Young, and E. W. V. Stryland, "Determination of bound-electronic and free-carrier nonlinearities in ZnSe, GaAs, CdTe, and ZnTe," J. Opt. Soc. Am. B **9**(3), 405–414 (1992).
52. P. Khan, A. R. Barik, E. M. Vinod, K. S. Sangunni, H. Jain, and K. V. Adarsh, "Coexistence of fast photodarkening and slow photobleaching in $Ge_{19}As_{21}Se_{60}$ thin films," Opt. Express **20**(11), 12416–12421 (2012).

1. Introduction

Chalcogenide glasses, based on S, Se or Te elements in combination with suitable elements from 14th or 15th group of the periodical system (Ge, As, Sb, etc.), are known to present high linear refractive index, photosensitivity to light exposure [1–4], and to be highly nonlinear [5–7]. Indeed, they present great Kerr nonlinearities at femtosecond time scale which can reach values several orders of magnitude larger than that of silica glass, variable two-photon absorption depending on their bandgap and insignificant free carrier absorption [8]. For these reasons, chalcogenide glasses have been studied under the scope of the development of all-optical signal processing based on nonlinear effects for telecommunication systems [9–13]. For mentioned integrated optical devices, a key prerequisite is an identification of appropriate bulk glass composition regarding the nonlinear figure of merit (FOM) for photonic applications. Thus, among the variety of chalcogenide glasses compositions, materials presenting high nonlinear refractive index represented by n_2 (m^2/W), low two photon absorption (TPA) defined by nonlinear absorption coefficient β (m/W), leading to optimized $FOM = \frac{n_2}{\lambda \beta_{TPA}}$, along with negligible linear absorption α (m^{-1}) are of interest. Given the diversity of vitreous compositions available, it is necessary to predict the overriding factors which could lead to the best figure of merit.

For crystalline semiconductors according to the theoretical works based on a two-band model assuming a sharp absorption edge proposed by Sheik-Bahae *et al.*, it was reported that TPA starts to occur when the photon energy (hν) is above the half bandgap energy E_g while

#203558 - $15.00 USD Received 23 Dec 2013; revised 18 Feb 2014; accepted 19 Feb 2014; published 25 Feb 2014

n_2 is an increasing function of photon energy until $h\nu = 0.5E_g$ in case of direct gap or close to E_g for indirect gap [14]. Consequently, the figure of merit fluctuates inside this energy range.

The sulfide and selenide glasses are considered as indirect gap amorphous materials and thus, the two-band model is not absolutely valid without a rough approximation [15]. The distribution of electronic states of amorphous semiconductors remains not perfectly described [16]. It can be noted that the exact determination of optical bandgap E_g, with no well-defined band edges due to the presence of tails and localized electronic states encroached up on the bandgap, is still subject of discussion. Consistent with the approximate onset of significant absorption, the optical gap E_g^{03} is generally taken at α = 1000 cm^{-1} for which the absorption changes from the one controlled by Tauc's relation (where the density of states can be approximated to parabolic bands of extended states) to an exponential Urbach's tail absorption involving both, tail states and extended states. As absorption coefficient is following Tauc's relation in region of $h\nu \geq E_g$, the optical gap E_g can be also evaluated from Tauc's law typically used in case of amorphous chalcogenide thin films.

The presence of Urbach's tail related to both, thermal effects and static disorder, leads to TPA below the half bandgap energy. Far below the bandgap energy, the linear properties, α and n_0 (linear refractive index), do not exhibit strong dependences on E_g; unlike the nonlinear properties [17]. Naturally for a given λ_{laser}, the TPA increases from sulfide glasses to selenide glasses following the bandgap energy decrease. In case of telecommunication wavelength, an energy bandgap larger than ~1.6 eV is required for a negligible TPA. Some increase of TPA in selenide glasses can be tolerated if n_2 is growing faster. Sanghera *et al.* used the classical anharmonic oscillator model to describe the nonlinear data and claimed a linear dependence of n_2 versus $\frac{1}{E_g^6} \cdot \frac{1}{(1-\left(\frac{h\nu}{E_g}\right)^2)^4}$ providing a predictive capability for nonlinear refractive index [8].

Moreover, if one considers a microscopic approach, the correlation between the local structure (polarity and covalent-ionic nature of the bonds) and the optical nonlinearities in chalcogenide glasses is not completely established yet. However, the polarizable electronic lone pairs (S, Se, As, Sb) seem to have a direct influence on the nonlinear refractive index. For high optical nonlinearities, As-S(Se,Te) and Ge-(As)-S(Se,Te) glass systems were mainly studied [18–22]. The substitution of S with Se or Te was realized in order to increase the n_2 from 2 to 7·10^{-18} m^2/W for As_2S_3 glass to 11-30·10^{-18} m^2/W for As_2Se_3 glass at near-infrared wavelengths, see for instance [19, 20, 23, 24]. Nevertheless, according to Harbold *et al.* [19, 20], nonlinear refractive index of sulfide and selenide glasses based on As-S(Se) and Ge-As-S(Se) systems is not only dependent on the lone pair electron density of the chalcogen and arsenic, but also on two-photon resonant enhancement accompanied by TPA when the photon energy of the operating laser approaches half of the optical bandgap energy of the material. Thus, in Ge-As-Se system for a fixed ratio of Ge/As = 0.5, a deficit of selenium, which decreases the electronic lone pair density, seems to increase n_2. It was shown that in Ge-As-Se glass set, where the normalized photon energy ($\frac{h\nu}{E_g}$) varies from 0.41 to 0.45, the highest value of n_2 was found for normalized photon energy equal to 0.45 with a major detrimental impact on the TPA following the bandgap energy decrease compared to stoichiometric composition. Consequently, the best FOM was obtained for the stoichiometric glass. In case of Ge-As-Se system glasses rich in Ge (Ge/As ratio varying from 1.1 to 2.8), Gopinath *et al.* [25] showed that variations of the nonlinear refractive index cannot be

#203558 - $15.00 USD Received 23 Dec 2013; revised 18 Feb 2014; accepted 19 Feb 2014; published 25 Feb 2014

satisfactorily explained considering the n_2 dependence on lone pair electron density. As the normalized photon energy varies only from 0.38 for stoichiometric glass to 0.41 for the glass with the highest deficit of selenium, the TPA is probably not really large for Ge rich glasses and β remains in the range of 0.4-0.5 cm/GW. Glasses with a strong deficit of Se present particular structure containing homopolar bonds (Ge(As)-Ge or As-As) that may possibly play a non-negligible role if one considers the microscopic approach.

We focused our attention on Ge-Sb-Se system regarding the substitution of As with Sb that may increase the nonlinear properties of the corresponding amorphous chalcogenides due to the enlargement of hyperpolarisability. The corresponding amorphous chalcogenides will have also lower bandgap energy related to this substitution. Further, the use of antimony is beneficial regarding its lower toxicity in comparison with arsenic. Finally, presence of antimony in amorphous chalcogenides is known to reduce photosensitivity of the material. Only few compositions were investigated in the Ge-Sb-Se system, $Ge_{28}Sb_{12}Se_{60}$ (commercially known as AMTIR-3 or IG5, E_g~1.8 eV) with $n_2 = 9.4 \cdot 10^{-18}$ m^2/W at 1.5 μm or some Se over-stoichiometric glasses for which the Ge/Sb varies from 1.1 to 5 measured at 1.064 μm [5, 26]. The tailoring of the glass chemical composition in Ge-Sb-Se system would lead to the optimization of FOM thanks to stronger increasing of n_2 comparing with TPA.

In this paper, beyond the description of basic physico-chemical properties we focused on nonlinear properties of selected bulk chalcogenide glasses from Ge-Sb-Se system. Within this ternary glass system, a careful analysis of trends in physico–chemical properties is performed by studying their compositional dependences along a characteristic cut-line of glass-forming region. Some authors claim that the knowledge of Z (mean coordination number reflecting the global connectivity of glass) and the glass composition (chemical short-range order) is needed to have a balanced view of the evolution of physico-chemical properties in ternary system [27]. In our case, we consider a variation of composition on the cut-line $(GeSe_2)_{100-x}(Sb_2Se_3)_x$ to investigate the introduction of antimony versus properties of glasses. Nonlinear refractive index and two-photon absorption of studied glasses are measured using Z-scan technique in picosecond regime at 1064 nm and at 1.55 μm in femtosecond regime using an original method. Photosensitivity of Ge-Sb-Se glasses is also studied at 1.55 μm in femtosecond regime.

2. Materials and experimental methods

For this study, chalcogenide glasses from pseudo-binary $(GeSe_2)_{100-x}(Sb_2Se_3)_x$ system (where x varied from 5 to 70) were synthesized. For reader's convenience, individual chemical compositions are shown in ternary Ge-Sb-Se diagram [Fig. 1, adopted from [28]]. Ge-Sb-Se glasses were prepared from commercial elements (Ge, Sb and Se) of high purity (5N) using the conventional melting and quenching technique. Despite the high purity of selenium, it presented a surface oxidation (SeO_2); therefore selenium was purified before mixing with other elements by distillations under dynamic and static vacuum. At first, all the elements were weighted in appropriate amounts, placed in a silica glass ampoule, which was evacuated and sealed. The elements were melted during 30 minutes at 850 °C in a rocking furnace. Then, the temperature was maintained at 800 °C during 10 hours. After quenching, glass rods were annealed 20 °C below their glass transition temperature during 6 hours, and finally slowly cooled down to room temperature. For optical characterization, resulting glass rods (25 mm diameter, 2mm in thickness) were sliced and polished (RMS roughness less than 3 nm as determined by atomic force microscopy measurements).

A scanning electron microscope with an energy-dispersive X-ray analyzer (EDS, JSM 6400-OXFORD Link INCA) was used for the determination of Ge-Sb-Se bulk glasses chemical composition and uniformity. Thermal characteristics of Ge-Sb-Se glasses were determined by DSC (Q20 DSC, TA Instruments). DSC measurements were performed with 10 mg powdered samples, heated up to 450°C at heating rate of 10 °C.min^{-1}.

#203558 - $15.00 USD Received 23 Dec 2013; revised 18 Feb 2014; accepted 19 Feb 2014; published 25 Feb 2014

The structure of bulk glasses was analyzed using micro-Raman spectroscopy. Raman spectra were recorded at room temperature under 785 nm laser excitation with an InVia reflex spectroscope (Renishaw) coupled to an Olympus BFXM free space x20 microscope.

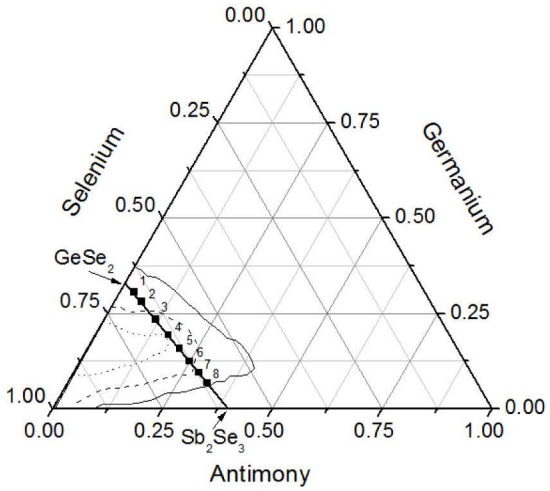

Fig. 1. Ternary diagram of Ge-Sb-Se system showing glass forming regions for different cooling rates (solid curve: water quenching, dashed curve: quenching on air, dotted curve: slow cooling), adopted from Popescu [28]. Synthesized $(GeSe_2)_{100-x}(Sb_2Se_3)_x$ samples are depicted by numbers, i.e. Nr. 1-8 stand for samples where x = 5, 10, 20, 30, 40, 50, 60, and 70. Samples Nr. 1-7 form glasses; sample Nr. 8 is of crystalline nature.

Transmittance spectra were measured with a visible-near-IR spectrophotometer (PerkinElmer). Linear refractive indices spectral dependencies (not shown here) as well as optical bandgap values of $(GeSe_2)_{100-x}(Sb_2Se_3)_x$ glasses were obtained from the analysis of variable angle spectroscopic ellipsometry (VASE) data measured using an ellipsometer with automatic rotating analyzer (J. A. Woollam Co., Inc.). The measurement parameters are as follows: spectral region 300-2300 nm with wavelengths steps of 20 nm, angles of incidence 50°, 60°, and 70°. For the analysis of VASE data, we used Cody-Lorentz model which includes both the correct band edge function and weak Urbach absorption tail; this model is appropriate for the description of amorphous chalcogenides optical functions [4].

Nonlinear refractive indices and two photon absorption coefficients were first measured using Z-scan technique [29] at 1064 nm [30]. The excitation is provided by a linearly polarized mode-locked Nd:YAG laser (1064 nm, pulse duration of 15 ps, 10 Hz). The measurement was performed using a 4f system. The image receiver is a 1000 x 1018 pixels cooled CCD camera (−30 °C) operating with a fixed gain. The sample is moved in the common focus region belonging to both lenses along the beam propagation direction (Z axis). Open and closed Z-scan normalized transmittance are numerically processed from the acquired images by integrating over all the pixels in the first case and over a circular numerical filter in the second one (giving a linear aperture transmittance equal to 0.7). The incident intensity can be varied by a polarizing system at the entry of the setup. In this work and when the material is highly absorbing, the intensity at the center of the beam and in the focus of the Z-scan system is kept around $I_0 = 0.4$ GW/cm^2.

Nonlinear optical properties of studied chalcogenide glasses were further determined in femtosecond regime. An optical parametric oscillator (OPO, Chameleon, Coherent Inc.) is tuned to 1.55 μm and focused in a bulk glass sample. Pulses duration is 200 fs, while repetition rate is 80 MHz, which gives peak power of 12.5 kW at the average output power of 200 mW. A NIR camera and two power meters monitor the output beam profile and sample

#203558 - $15.00 USD Received 23 Dec 2013; revised 18 Feb 2014; accepted 19 Feb 2014; published 25 Feb 2014

transmission, respectively. Both, two photon absorption coefficient and nonlinear Kerr coefficient, are deduced from direct transmission analysis (DTA). The TPA coefficients β are deduced from the analysis of samples transmission as a function of beam intensity. For this measurement, the beam waist is positioned mid-way between the entrance and output faces of the sample (typically 2 mm long) to minimize the influence of diffraction and self-focusing. In a second step, the beam waist is placed exactly at the entrance face of the sample and beam profile at the output face is monitored with the camera. From the modifications of the output beam diameter between linear and nonlinear regime, the Kerr coefficient n_2 sign and amplitude are deduced. To this end, the experimental observations are compared with simulations based on numerical resolution of the nonlinear Schrödinger equation. Moreover, from the same experimental arrangement, the damage threshold intensities are evaluated for the different glass compositions. At last, to study the photosensitivity of the materials, the long term evolution of the beam profile at the exit face of the chalcogenide samples is observed.

3. Results and discussion

3.1 Physico-chemical properties

The bulk $(GeSe_2)_{100-x}(Sb_2Se_3)_x$ samples were amorphous, as confirmed by X-ray diffraction patterns, excluding $(GeSe_2)_{30}(Sb_2Se_3)_{70}$ material, which contains crystals and was not used for further structural and optical characterization. Chemical composition of fabricated $(GeSe_2)_{100-x}(Sb_2Se_3)_x$ glasses as determined using EDS is in good agreement with nominal one; the differences are about 1 at. % - this value corresponds to the EDS measurements uncertainty (Table 1). Table 1 contains also cut-off wavelengths showing linear increase with introduction of Sb_2Se_3. The bandgap energy determined by Cody-Lorentz model from VASE data (± 0.01 eV) decreases with introduction of Sb_2Se_3 in good agreement with E_g^{03} values.

Table 1. Theoretical and real chemical composition (evaluated by EDS) of fabricated $(GeSe_2)_{100-x}(Sb_2Se_3)_x$ glasses (± 0.5 at.%), their cut-off wavelengths determined as wavelengths at which absorption coefficient is equal to 10 and 1000 cm^{-1}, and optical bandgap (E_g, ± 0.01 eV) values extracted by Cody-Lorentz model from VASE data and as energy where α = 1000 cm^{-1} (E_g^{03}).

Sample	Theoretical comp. (at. %)	Real comp. (at. %)	$\lambda_{cut-off}$ (nm)		E_g (eV)	
			$10cm^{-1}$	10^3cm^{-1}	C-L	E_g^{03}
x=5	$Ge_{30.6}Sb_{3.2}Se_{66.1}$	$Ge_{31.0}Sb_{3.4}Se_{65.6}$	678	558	2.17	2.22
x=10	$Ge_{28.1}Sb_{6.3}Se_{65.6}$	$Ge_{28.3}Sb_{6.8}Se_{64.9}$	689	574	2.11	2.16
x=20	$Ge_{23.5}Sb_{11.8}Se_{64.7}$	$Ge_{23.1}Sb_{13.0}Se_{63.9}$	749	613	2.02	2.02
x=30	$Ge_{19.4}Sb_{16.7}Se_{63.9}$	$Ge_{19.5}Sb_{17.8}Se_{62.7}$	792	656	1.86	1.89
x=40	$Ge_{15.8}Sb_{21.1}Se_{63.2}$	$Ge_{14.9}Sb_{22.3}Se_{62.8}$	843	694	1.78	1.79
x=50	$Ge_{12.5}Sb_{25}Se_{62.5}$	$Ge_{12.1}Sb_{25.5}Se_{62.5}$	885	728	1.70	1.70
x=60	$Ge_{9.5}Sb_{28.6}Se_{61.9}$	$Ge_{10.4}Sb_{29.1}Se_{60.5}$	934	764	1.54	1.62
x=70	$Ge_{6.8}Sb_{31.8}Se_{61.4}$	Crystallized	-	-	-	-

No crystallization peaks were observed in DSC curves (in measured temperature region) except for x = 70 composition which is close to glassy domain edge [Fig. 1]. Globally, glass transition temperature (T_g) decreases monotonously when antimony concentration increases [Fig. 2]. This trend follows changes of vitreous network connectivity occurring when antimony is incorporated in chalcogenide glasses. We note that antimony coordination is 3 (in $[SbSe_{3/2}]$ pyramids), whereas germanium is known to be in a tetrahedral environment ($[GeSe_{4/2}]$ tetrahedra). On the other hand, density of $(GeSe_2)_{100-x}(Sb_2Se_3)_x$ glasses clearly increases with rising x [Fig. 2]. Considering atomic masses of elements (A_r(Ge) = 72.64, A_r(Sb) = 121.76, A_r(Se) = 78.96)), the density of glasses increases coherently with antimony introduction.

#203558 - $15.00 USD Received 23 Dec 2013; revised 18 Feb 2014; accepted 19 Feb 2014; published 25 Feb 2014

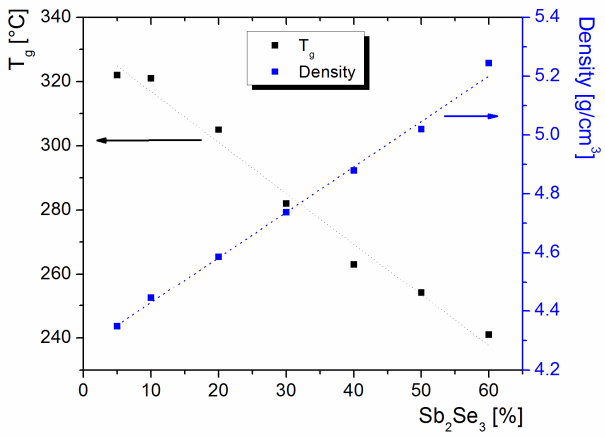

Fig. 2. Compositional dependences of glass transition temperature (T_g) and density of $(GeSe_2)_{100-x}(Sb_2Se_3)_x$ glasses (x = 5-60).

3.2 Structure of $(GeSe_2)_{100-x}(Sb_2Se_3)_x$ glasses

Raman study of amorphous selenium [31] and amorphous germanium [32] have been reported in the last 60s. Concerning Ge-based chalcogenide glasses, a lot of published data report on amorphous (a-) $GeSe_2$ structure [33–37] and to less extent on more complex system, such as ternary and quaternary glasses [38–42]. Table 2 summarizes the main features observed in the Raman scattering spectra and their attribution, according to past studies.

Table 2. Contributions of different structural entities to Raman scattering spectra in Ge-Sb-Se glasses according to past studies.

ν (cm^{-1})		Vibration mode	Environment	Reference
285-300	(1)	F_2 asym. vibration mode	$GeSe_4$	[33, 42, 43]
265	(3)	A_1 mode	Se_n chains $[GeSe_{4/2}]$ corner linked (dimers, small chains)	[34, 38, 41, 42] [39, 40]
240-250	(4)	A_1 mode	Se_n rings	[31, 38, 41]
245		stretching mode	Se-Se at the outrigger	[42]
235		A_1 mode	Se_n chains in a-Se	[31, 40]
215	(5)	A_1^c breathing companion mode	$[GeSe_{4/2}]$ connected by edge	[35-37, 41, 42]
200	(6)	A_1 sym. stretching mode	$[GeSe_{4/2}]$ connected by corner	[35, 36, 38, 41, 42]
190	(7)	Sb-Se bond stretching mode	$[SbSe_{3/2}]$ pyramids	[40, 41, 44]
170 270	(8) (2)	Ge-Ge bond vibration	$Ge_2Se_{6/2}$ $Ge\text{-}Ge_mSe_{4-m}$ m = 1,2,3,4	[32, 36, 37, 40]
155	(9)	Sb-Sb	$Se_2Sb\text{-}SbSe_2$	[38, 40, 44]
145		bending mode	Se-Se at the outrigger	[34]
138	(10)	rotational vibration mode	Se polymeric chains	[31]

Normalized Raman scattering spectra of bulk $(GeSe_2)_{100-x}(Sb_2Se_3)_x$ glasses are presented in Fig. 3. For a comparison, Raman spectrum of $GeSe_2$ glass is shown as well.

Normalized Raman spectra were decomposed using ten Gaussian contributions corresponding to ten vibrational modes observed in the glassy matrix and numbered in Table 2. As an example, Fig. 4 shows decomposition of $(GeSe_2)_{90}(Sb_2Se_3)_{10}$, $(GeSe_2)_{70}(Sb_2Se_3)_{30}$, and $(GeSe_2)_{50}(Sb_2Se_3)_{50}$ Raman spectra.

#203558 - $15.00 USD Received 23 Dec 2013; revised 18 Feb 2014; accepted 19 Feb 2014; published 25 Feb 2014

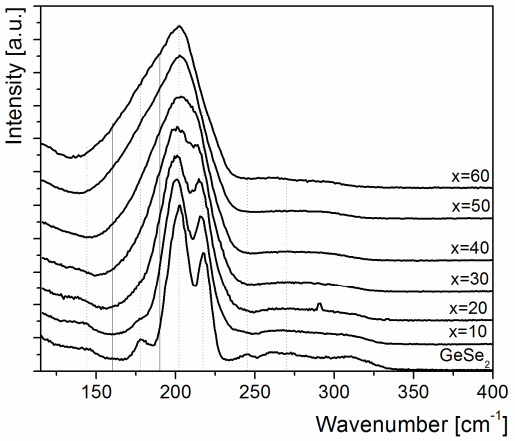

Fig. 3. Raman scattering spectra of bulk $(GeSe_2)_{100-x}(Sb_2Se_3)_x$ glasses (x = 0-60). Dotted lines correspond to contributions coming from Ge-Se structural entities, solid lines correspond to contributions due to introduction of antimony.

The dominant feature of the spectra of $GeSe_2$-rich glasses is a broad band in the ~170-240 cm^{-1} spectral region. Two main peaks are observed at ~200 and ~215 cm^{-1} which are attributed to A_1 symmetric stretching mode of corner linked $[GeSe_{4/2}]$ tetrahedra and to A_1^c breathing vibration mode (also called companion mode) of $[GeSe_{4/2}]$ tetrahedra connected by edge. In a-$GeSe_2$, a 170 cm^{-1} contribution is observed, which, associated with a weaker 270 cm^{-1} contribution, is revealing Ge-Ge bonds vibrations. In detail, Raman feature peaking at ~170 cm^{-1} is significant for $Ge_2Se_{6/2}$ entities and band with maximum at ~270 cm^{-1} is assigned to Ge-Ge_mSe_{4-m} (m = 1,2,3,4) entities. One can also note a broad band of low intensity, covering ~230-330 cm^{-1} region which corresponds to homopolar Se-Se bonds originating from different kind of entities (Se chains at ~235 cm^{-1}, stretching mode of Se-Se bond at the outrigger at ~245-250 cm^{-1}, $[GeSe_{4/2}]$ corner-shared dimers at ~265 cm^{-1}). At higher frequencies (i.e. ~285-300 cm^{-1}), one can expect a contribution of F_2 asymmetric vibration mode of $[GeSe_{4/2}]$ tetrahedra.

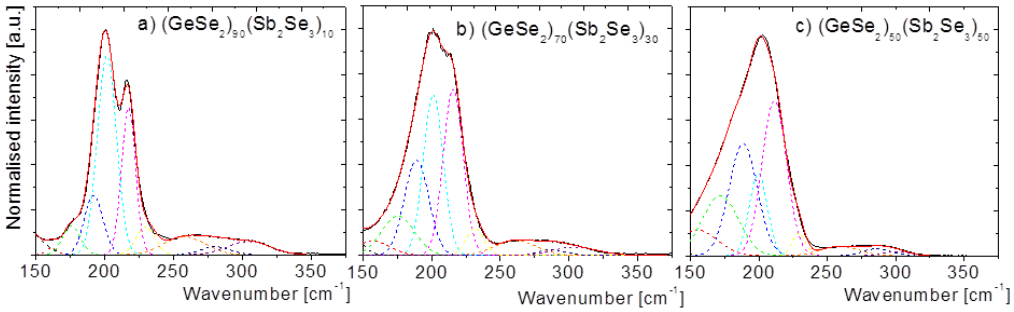

Fig. 4. Raman scattering spectra of $(GeSe_2)_{90}(Sb_2Se_3)_{10}$ (a), $(GeSe_2)_{70}(Sb_2Se_3)_{30}$ (b), and $(GeSe_2)_{50}(Sb_2Se_3)_{50}$ (c) glasses, and their respective decomposition in Gaussian curves (colored dashed lines). Full red curves correspond to the sum of Gaussian contributions.

When increasing Sb content in the glassy matrix, changes in Raman spectra are observed. First of all, intensities of Raman bands peaking at ~200 and ~215 cm^{-1} decrease with increasing Sb content. Looking at decomposition of Raman spectra [Fig. 4], one can note that the ratio between the intensity of the A_1 and the A_1^c contributions decreases with increasing

#203558 - $15.00 USD Received 23 Dec 2013; revised 18 Feb 2014; accepted 19 Feb 2014; published 25 Feb 2014

Sb content, meaning that corner linked tetrahedra are the first bonds broken by Sb introduction. The network slowly evolves from a tetrahedra dominated network to a pyramidal one. Peak intensity corresponding to Ge-Ge bonds vibrations (~170 and ~270 cm^{-1}) also decreases when Sb content increases. Raman intensity at ~140 cm^{-1} which is significant for a type E vibrational mode of Se polymeric chains, decreases when Sb content increases. Finally, a broadening of the main band is observed; this broadening is due to the increase of ~190 cm^{-1} contribution corresponding to Sb-Se bond vibration in [$SbSe_{3/2}$] pyramids. A Raman feature peaking at ~160 cm^{-1} appears when Sb_2Se_3 content reaches 40%, corresponding to Sb-Sb bond vibration in Se_2Sb-$SbSe_2$ entities. Note that the Ge-based entities in this region (at ~170 cm^{-1}) are dominated by the Sb-based entities, probably due to their higher polarizability, leading to masking effects, as observed in case of Ge-Sb-Te and Ge-Sb-S system [45, 46]. The broad high frequency band of low intensity (~230-330 cm^{-1}) also tends to disappear when increasing Sb content, meaning that its introduction induces probably a diminution of homopolar Se-Se bond in the glassy matrix.

In order to understand in more detail structural changes occurring in $(GeSe_2)_{100-x}(Sb_2Se_3)_x$ glasses with increasing Sb_2Se_3 content, relative intensities of vibrational modes were investigated as follows. The Sb_2Se_3 content dependence of the intensity ratio of the A_1^c to the A_1 modes was plotted, corresponding qualitatively to the ratio between number of edge-sharing tetrahedra to corner-sharing ones present in the glassy matrix [Fig. 5]. In Ge rich Ge_xSe_{1-x} glasses, the formation of edge-sharing polyhedra is favored, as observed by Sugai [35]. As shown in Fig. 5, intensity ratio of edge-shared to corner-shared entities increases with x. Decrease of $GeSe_2$ component concentration in the glassy network thus tends to favor presence of edge-shared [$GeSe_{4/2}$] tetrahedra and to reduce the number of corner-shared [$GeSe_{4/2}$] tetrahedra within the network, in agreement with Petit's study [26]. Glasses rich in Sb_2Se_3 thus contain a large number of $Ge_2Se_{8/2}$ entities. Furthermore, number of Se-Se bonds slowly increases compare to Ge-Se bonds from edge and corner-shared tetrahedra [Fig. 5]. Intensity ratio of Ge-Ge vibrational mode located at ~170 cm^{-1} ([$Ge_2Se_{6/2}$] entities) to the sum of edge and corner-shared Ge-based tetrahedra also slightly increases when Sb_2Se_3 content is higher than 30%. Introduction of Sb_2Se_3 will then favor formation of homopolar Ge-Ge and Se-Se bonds at the expense of Ge-Se bonds. Intensity ratio of Raman 270 cm^{-1} feature (assigned to Ge-Ge_mSe_{4-m} structural motifs) to 170 cm^{-1} feature (attributed to $Ge_2Se_{6/2}$ entities) decreases with increasing content of Sb, leading to the conclusion that the formation of [$Ge_2Se_{6/2}$] entities may be preferred when introducing Sb into glassy structure. Note that for higher Sb_2Se_3 content in the glasses, calculated intensities of individual contributions suffer due to higher uncertainties coming from global shape of the spectra. Finally, intensity ratio of Raman 155 cm^{-1} band (Sb-Sb bonds vibrations) to 190 cm^{-1} feature (Sb-Se vibrations) slightly increases when increasing Sb_2Se_3 content [Fig. 5]. Thus, Sb-Sb bonds may be preferentially formed at high Sb concentrations in $(GeSe_2)_{100-x}(Sb_2Se_3)_x$ glasses.

To conclude, $GeSe_2$ glassy network is composed mainly of $GeSe_{4/2}$ units linked by corner or edge. Introduction of Sb_2Se_3 in the amorphous matrix seems to induce a progressive change in the network, first favoring edge-shared [$GeSe_{4/2}$] entities. Then, at intermediate Sb_2Se_3 contents, glassy network contains significant number of [$SbSe_{3/2}$] pyramids. Finally, at high Sb concentration in $(GeSe_2)_{100-x}(Sb_2Se_3)_x$ glasses, Se_2Sb-$SbSe_2$ structural motifs seems to be present.

Evolution of n_2 values in a system can be related to structure of the glass. As proposed by Harbold, nonlinear refractive index is not only dependent on lone pair electron concentration but mainly also on bandgap energy [19]. One can assume that change in nonlinear properties depends on the composition and structure of the glass, related to bandgap energy variation from one glass to another one. Petit *et al.* first demonstrated that in Ge-Sb sulfo-selenide glasses, the increase in nonlinear refractive index could be attributed to the increase of number of Sb-Se and Ge-Se bonds [47]. A more recent study of ternary Ge-Sb-Se glasses

#203558 - $15.00 USD Received 23 Dec 2013; revised 18 Feb 2014; accepted 19 Feb 2014; published 25 Feb 2014

[26] reported that n_2 of Se over-stoichiometric glasses, from $Ge_{23}Sb_7Se_{70}$ to $Ge_{16}Sb_{14}Se_{70}$, increases when Sb/Ge ratio increases for a Se fixed composition.

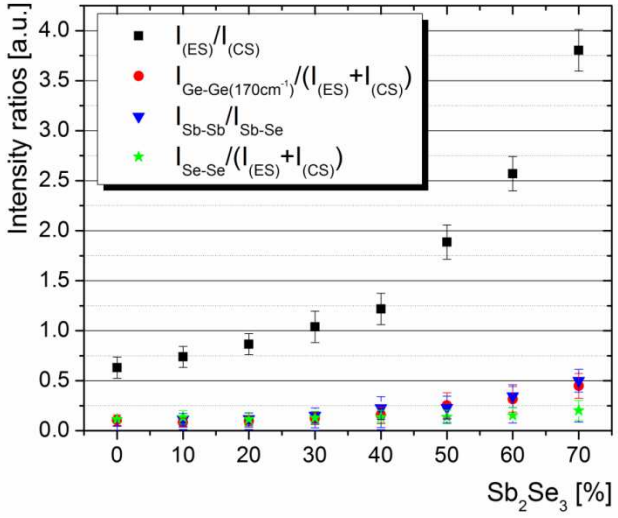

Fig. 5. Intensity ratios for various Raman active vibration modes. $I_{Se\text{-}Se}$ corresponds to the sum of ~230 and ~260 cm^{-1} contributions from homopolar Se-Se bonds. I_{ES} and I_{CS} are intensities of A_1^c and A_1 bands, respectively (ES is for edge-shared and CS for corner-shared tetrahedra). $I_{Sb\text{-}Sb}$ and $I_{Sb\text{-}Se}$ correspond to ~155 cm^{-1} and ~190 cm^{-1} contributions, respectively.

It should be mentioned that the number of Se-Se bonds is slightly increasing when the Sb/Ge increases, which can also play a secondary role for n_2. Nevertheless, in case of $Ge_{(13+x)}Sb_7Se_{80-x}$ (x = 0, 10, 15, 22) glass set, the Ge/Sb ratio increase induces an increase of n_2 until the composition becomes Se under-stoichiometric, for which the presence of Ge-Ge homopolar bonds starts to be not negligible and the $[GeSe_{4/2}]$ edge linked tetrahedra content stops to increase. The two main effects of Ge/Sb increase in discussed over-stoichiometric glass set is the increase of $[GeSe_{4/2}]$ tetrahedra number connected by edges compare to those connected by corners and the decrease of number of Se-Se bonds. It was also shown that n_2 value is related to the number of heteropolar bonds within the glassy matrix and is more influenced by the increase of Sb-Se bonds number than by the increase of Ge-Se ones [26].

3.3 Nonlinear optical properties

Nonlinear characterization of studied Ge-Sb-Se glasses are first studied in picosecond regime using the Z-scan technique at 1.064 µm. Results are summarized in Table 3 together with results obtained at 1.55 µm in femtosecond regime. For a comparison, nonlinear characteristics of classical chalcogenide compositions (As_2S_3, As_2Se_3, and $Ge_{28}Sb_{12}Se_{60}$ glasses) measured by other authors are included in Table 3 as well. Linear refractive indices (calculated by VASE) are also shown.

Qualitatively, substitution of sulfur by selenium in chalcogenide glasses leads to a significant increase of n_2 values. The values of n_2 presented in this work are in good agreement with data measured by Petit *et al.* at 1.064 µm for $Ge_{28}Sb_7Se_{65}$ glass using a similar picosecond laser source [26]. Concerning the determination of two photon absorption coefficient at 1.064 µm, it is globally growing in studied $(GeSe_2)_{100-x}(Sb_2Se_3)_x$ glasses with increasing content of antimony which is in accordance with the shift of the bandgap to lower energies. One can find large discrepancies between individual values of two photon absorption coefficient (Table 3): β~0.2-2.0 and ~4.4-19.0 $cm.GW^{-1}$ at 1.064 µm for As_2S_3 and As_2Se_3 glasses, respectively. Among studied $(GeSe_2)_{100-x}(Sb_2Se_3)_x$ glasses, the highest FOM was found for $(GeSe_2)_{90}(Sb_2Se_3)_{10}$ composition, reaching value of ~1.2, which is

#203558 - $15.00 USD Received 23 Dec 2013; revised 18 Feb 2014; accepted 19 Feb 2014; published 25 Feb 2014

significantly larger comparing with other Ge-Sb-Se glasses measured at 1.064 µm. Nevertheless, the measured β values seem to be overestimated compared to value obtained at 1.55 µm, decreasing strongly the FOM at 1.064 µm.

Table 3. Linear (n_0) and nonlinear (n_2) refractive indices, $n_2/n_2(SiO_2)$ ratios, two photon absorption coefficients (β), nonlinear figures of merit (FOM) of $(GeSe_2)_{100-x}(Sb_2Se_3)_x$ glasses determined at 1.064 and 1.550 µm. For a comparison, data for $Ge_{28}Sb_{12}Se_{60}$, As_2Se_3, and As_2S_3 glasses taken from other authors are given. Note that literature data could differ from this work in measurement method and measurement wavelength (MZI is for Mach-Zehnder interferometry, SRTBC is for spectrally resolved two-beam coupling).

Sample	n_0	n_2 (10^{-18} m^2.W^{-1})	n_2/n_{2SiO2}	β (cm.GW^{-1})	*FOM*	Method	λ (µm)	Ref.
x = 5	2.46	7.0 ± 1.2	233	1.9 ± 0.5	0.35	Z-scan	1.064	This work
	2.42	6.5 ± 2.0	241	0.44	0.95	DTA	1.550	
x = 10	2.51	8.9 ± 2.7	297	< 0.7	1.19	Z-scan	1.064	This work
	2.47	9.0 ± 2.0	333	0.29	2.00	DTA	1.550	
x = 20	2.61	9.1 ± 1.8	303	2.3 ± 0.5	0.24	Z-scan	1.064	This work
	2.56	9.6 ± 2.0	356	0.32	1.90	DTA	1.550	
x = 30	2.73	14.1 ± 2.9	470	10.5 ± 1.4	0.13	Z-scan	1.064	This work
	2.67	9.97 ± 2.0	369	0.31	1.90	DTA	1.550	
x = 40	2.85	14.8 ± 2.9	493	12.4 ± 1.8	0.11	Z-scan	1.064	This work
	2.78	14.3 ± 3.0	530	NA	NA	DTA	1.550	
x = 50	2.97	17.7 ± 5.9	590	21.4 ± 4.1	0.08	Z-scan	1.064	This work
	2.89	20.3 ± 3.0	752	0.84	1.60	DTA	1.550	
x = 60	3.10	21.2 ± 4.6	707	21.5 ± 2.3	0.09	Z-scan	1.064	This work
	3.01	NA	NA	1.01	NA	DTA	1.550	
$Ge_{28}Sb_{12}Se_{60}$		9.4	350	NA	3.00	Z-scan	1.5	[5]
	2.72	13.7 ± 2.2	457	7.5 ± 0.95	1.72	Z-scan	1.064	This work
As_2Se_3	2.90	19 ± 3	633	19.0 ± 3	0.1	Z-scan	1.064	This work
		14 ± 3.5	540	4.4 ± 1.1	0.30	MZI	1.064	[48]
		18	690	4.5	0.38	Z-scan	1.064	[6]
		30 ± 4.5	1200	2.8 ± 0.4	0.86	SRTBC	1.25	[20]
		19	500	NA	2	Z-scan	1.5	[5]
As_2S_3		4.3 ± 1.1	170	0.2 ± 0.05	2.02	MZI	1.064	[48]
		2.5 ± 0.2	100	2.0 ± 0.14	0.12	Z-scan	1.064	[23]
		6.8 ± 1.0	260	0.16 ± 0.02	3.40	SRTBC	1.25	[20]

Nonlinear properties of studied glasses at 1.55 µm have been investigated using the setup described above. TPA coefficients have first been evaluated by fitting the measured samples transmission T as a function of the input beam intensity I_0 using Eq. (1):

$$T = \frac{\exp(-\alpha L)}{1 + \beta I_0 \left(\frac{1 - \exp(-\beta L)}{\alpha} \right)}. \quad (1)$$

In Eq. (1), α is the linear absorption coefficient and L is the sample thickness. Deduced values for β are reported in Table 3. Note that, as expected, TPA is lower than at 1.06 µm.

The technique to evaluate the Kerr coefficient at 1.55 µm is based on the analysis of the beam profile variation when the nonlinear effect is present. In linear regime, beam size enlarges due to diffraction over propagation while in nonlinear regime, i.e. at high laser power, the Kerr effect can either further defocus the beam (n_2<0) or gives some focusing (n_2>0).

For the experiment, the laser beam from the OPO tuned at 1.55 µm is focused to (typically) 26 µm FWHM spot at the entrance face of the sample to be analyzed. In the studied Ge-Sb-Se glasses, a clear decrease of the beam size diameter is observed at the output

#203558 - $15.00 USD Received 23 Dec 2013; revised 18 Feb 2014; accepted 19 Feb 2014; published 25 Feb 2014

face at high power compare to low power, as illustrated in Fig. 6. It shows unambiguously that n_2 is positive.

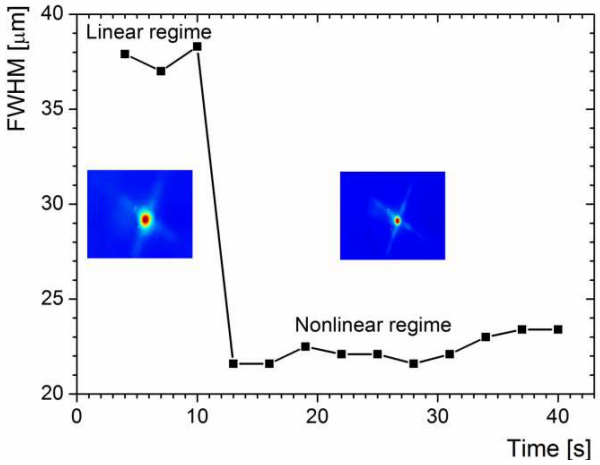

Fig. 6. Measured evolution of beam FWHM at the output of a 2.21 mm long $(GeSe_2)_{60}(Sb_2Se_3)_{40}$ sample when input light beam intensity is switched from linear regime to nonlinear regime (I_0 = 1.4 GW/cm^2) at t = 10 s. Inserts show two corresponding observed images.

Furthermore, n_2 values at 1.55 μm are determined by comparison of experimental beam self-focusing observations with predictions obtained by numerical solution of the nonlinear Schrödinger equation. As an illustration, Fig. 7 shows the calculated beam size (FWHM) at the exit face of a 2.26 mm long chalcogenide glass as a function of the n_2 coefficient for a 25.7 μm FWHM input beam for two different input intensities.

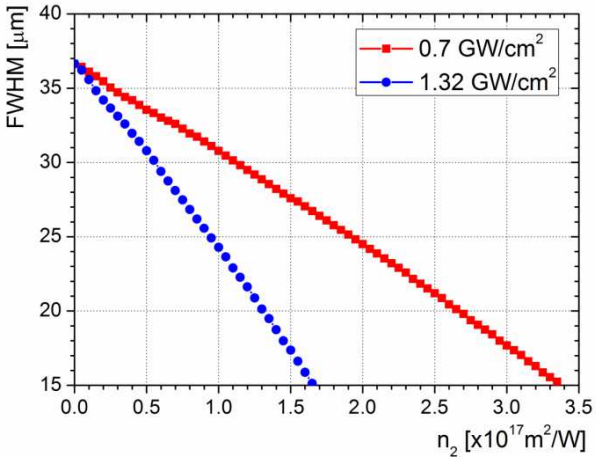

Fig. 7. Calculated output beam FWHM as a function of the nonlinear refractive index n_2 for two different input light intensities I_0. Parameters: $(GeSe_2)_{95}(Sb_2Se_3)_5$ glass, input FWHM = 25.7 μm, sample length = 2.26 mm, linear refractive index = 2.42, λ = 1550 nm, α = 0.15 cm^{-1}, β = 0.44 cm/GW.

For studied glasses, significant beam size change is thus predicted between linear (n_2 = 0) and nonlinear regime. To accurately determine n_2, linear loss and evaluated TPA are also taken into account in the simulations. The deduced n_2 values are presented in Table 3. It shows that Kerr effect is stronger in glass with higher Sb_2Se_3 content and β coefficient follows the same trend. *FOM* as high as 1.9-2.0 can be reached for intermediate

#203558 - $15.00 USD Received 23 Dec 2013; revised 18 Feb 2014; accepted 19 Feb 2014; published 25 Feb 2014

compositions. For $(GeSe_2)_x(Sb_2Se_3)_{100-x}$ glasses with $5<x<50$, estimated values of n_2 coefficient vary from $6.5\cdot10^{-18}$ to $2.0\cdot10^{-17}$ $m^2.W^{-1}$ at 1.55 µm. This is in good agreement with data measured for $Ge_{28}Sb_{12}Se_{60}$ glass by Lenz *et al.* at 1.5 µm using a similar femtosecond laser source [5]. The n_2 of Ge-Sb-Se glasses are at least 20% larger than those of Ge-As-Se glasses of analogous stoichiometric composition; that is to say $Ge_{25}As_{10}Se_{65}$ and $Ge_{12.5}As_{25}Se_{62.5}$ ($n_2 = 6.0\cdot10^{-18}$ and $1.7\cdot10^{-17}$ $m^2.W^{-1}$) [19, 25]. Note that an accurate n_2 value could not be measured in glass with the highest Sb_2Se_3 content due to poor reproducibility of the measurements. Within Ge-Sb-Se system, we show that an increase of antimony clearly leads to increasing values of the nonlinear refractive indices; n_2 at 1.55 µm is estimated to be up to ~750 times the value of fused silica ($n_2(SiO_2)\sim0.027\cdot10^{-18}$ $m^2.W^{-1}$) [49]. Regarding structural evolution of Ge-Sb-Se glasses with addition of antimony, one can associate the increase in nonlinear refractive index values, as observed by Petit *et al.* [26], mainly to the increase in Sb-Se bonds number.

Damage peak intensity thresholds of studied glasses have also been assessed using the same optical set-up at 1.55 µm with pulses duration of 200 fs. It spans to about 2.5 $GW.cm^{-2}$ for low Sb content glasses down to 1.6 $GW.cm^{-2}$ for $(GeSe_2)_{40}(Sb_2Se_3)_{60}$.

From the values reported in Table 3, we note that there are usually large discrepancies between n_2 values obtained for the same glass composition (for example $14\text{-}30\cdot10^{-18}$ $m^2.W^{-1}$ in case of As_2Se_3 glass) obtained by different measurement techniques (Z-scan, Mach-Zehnder interferometry or spectrally resolved two-beam coupling). The uncertainty of the measurement techniques and probably the different glass purities (which may affect transmission and bandgap energy) can also induce discrepancies in n_2 values. Moreover, the deduced n_2 and β values also depend on the incident intensity due to several features such as free carrier refraction and absorption changes [50] and possible higher order nonlinearities as intensity rises. These are sources of errors when evaluating nonlinear coefficients. Experimentally it is demonstrated that there is a decrease of the effective nonlinear coefficients with increasing intensity. This behavior has also been seen in crystalline semiconductors [51].

3.4 Photoinduced effects

Additionally to the instantaneous self-focusing due to the Kerr effect, a slow and irreversible variation of the output beam size can be observed for some glass compositions at high intensity when illumination time is long. To quantify this effect, the same optical arrangement as for the evaluation of the Kerr coefficient is used. Figure 8 shows the time evolution of the output beam FWHM normalized to the initial FWHM in different $(GeSe_2)_{100-x}(Sb_2Se_3)_x$ glasses when illuminated with intensities of about half the peak intensity damage threshold.

In the $(GeSe_2)_{95}(Sb_2Se_3)_5$ glass, the output beam FWHM does not evolve significantly over the observation time of 80 minutes. The absence of photosensitivity is not surprising due to the large energy bandgap of this composition compare to the photon energy. To the contrary, for $(GeSe_2)_{90}(Sb_2Se_3)_{10}$ and $(GeSe_2)_{80}(Sb_2Se_3)_{20}$ glasses, a gradual self-focusing is clearly observed. In the latter composition, it even leads to a 15 µm FWHM spot at the output face of the sample which is remarkably smaller than the one at the entrance face (26 µm). This photosensitivity is thus associated with an increase of the index of refraction in the illuminated area. At the end of the photoinduced process, the beam size slightly enlarges when the laser beam power is reduced but a permanent self-focusing persists. This irreversible self-focusing effect is attributed to a permanent photoinduced refractive index change that adds up to the Kerr effect. Remarkably, as the Sb_2Se_3 content is further increased, the permanent self-focusing tends to disappear and even changes to a defocusing effect for highest Sb_2Se_3 content. For instance, $(GeSe_2)_{70}(Sb_2Se_3)_{30}$ composition shows no discernible change in beam size while experiments with $(GeSe_2)_{60}(Sb_2Se_3)_{40}$ glass reveal an increasing

#203558 - $15.00 USD Received 23 Dec 2013; revised 18 Feb 2014; accepted 19 Feb 2014; published 25 Feb 2014

output beam FWHM over time which is the sign of a defocusing effect due to the photosensitivity. We also note that the irreversible index change becomes weaker and appears slower in any composition for lower laser power. Beam size change is unnoticeable at an average power lower than 50 mW (intensity of about 0.3 GW.cm^{-2}). Moreover, it is important to note that no photosensitivity is observed if a CW source with the same average power of 200 mW and the same wavelength as the femtosecond laser is used. This leads to the conclusion that the photosensitivity is not related to thermal effects but to optical nonlinearities.

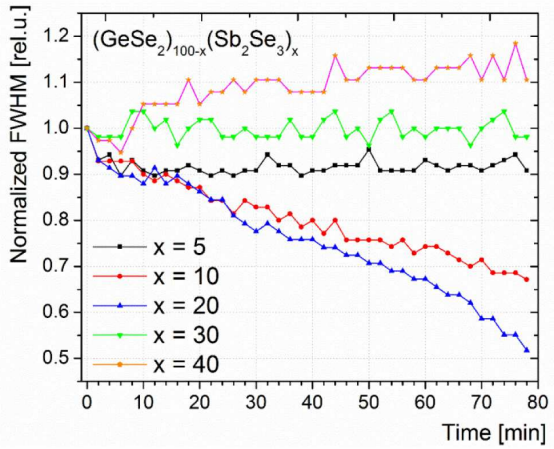

Fig. 8. Evolution of output beam size with time for $(GeSe_2)_{100-x}(Sb_2Se_3)_x$ glasses for intensities I_0 of about 1.8 GW/cm^2 (x = 5), 1.5 GW/cm^2 (x = 10 and x = 20), 1.3 GW/cm^2 (x = 30), and 1.1 GW/cm^2 (x = 40).

We thus observed an evolution of the output beam size in nonlinear regime for long interaction time (80 min) which is very dependent on glass composition. The experiments suggest that the irreversible index variations are related to nonlinear absorption that gives either photodarkening in self-focusing medium or photobleaching in self-defocusing medium. To confirm this hypothesis, samples transmission T in nonlinear regime is studied over time. The experimental setup is slightly modified with the insertion of two powermeters, one to monitor the input power and the other one for the output power. Evolution of the transmission, normalized to the initial one (T_0), of three characteristic glass compositions is presented in Fig. 9 for peak intensities similar to Fig. 8.

First, we observe that a fast dynamic is present at the beginning of the transmission curves. Indeed, in few seconds after switching on irradiating laser, a fast increase of the transmission is observed. These fast transmission variations could be due to defects leading to charge carrier trapped in localized levels; after the first few seconds, localized levels could no longer lead to a two-photon absorption limiting transmission. After described fast transmission increase, weak variations of transmission are also observed on a longer time scale. A decrease in transmission is observed in the case of self-focusing samples (for example $(GeSe_2)_{80}(Sb_2Se_3)_{20}$ glass) while an increase of transmission is observed in the case of self-defocusing sample ($(GeSe_2)_{50}(Sb_2Se_3)_{50}$). This is consistent with a photodarkening effect frequently associated with an increase of the refractive index whereas photobleaching is usually accompanied with a decrease of the index. Note that for the focusing samples, burning of the input glass surface is observed experimentally when illumination time approaches 80 min. This damage is certainly due to the increase of absorption connected with photodarkening. At last, intermediate compositions close to $(GeSe_2)_{70}(Sb_2Se_3)_{30}$ do not show any significant slow transmission evolution with time [Fig. 9] which is in agreement with observations made for beam profile analysis [Fig. 8] where only weak change in beam size (if

#203558 - $15.00 USD Received 23 Dec 2013; revised 18 Feb 2014; accepted 19 Feb 2014; published 25 Feb 2014

any) was observed. Note that the double kinetic observed in our sample transmission has also been recently reported in Ge-As-Se thin films. A fast transient photodarkening and a slower photobleaching effect were reported [52]. To better understand the behavior observed in our samples, a more complete study on structural properties of irradiated samples is under progress.

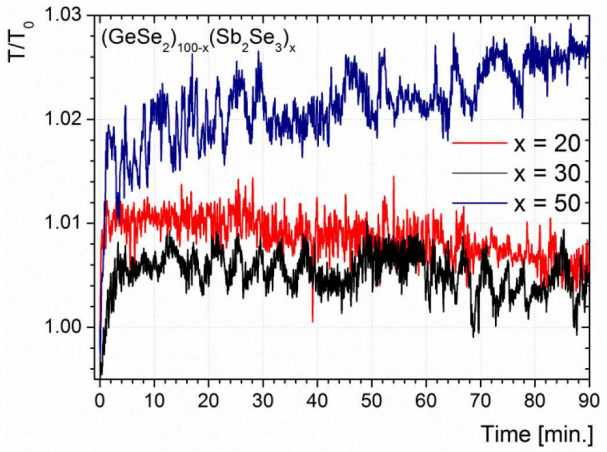

Fig. 9. Evolution of normalized transmission of $(GeSe_2)_{80}(Sb_2Se_3)_{20}$, $(GeSe_2)_{70}(Sb_2Se_3)_{30}$, and $(GeSe_2)_{50}(Sb_2Se_3)_{50}$ glasses. Intensities I_0 are 1.5 GW/cm^2 (x = 20), 1.3 GW/cm^2 (x = 30), and 0.9 GW/cm^2 (x = 50).

4. Conclusion

Physico-chemical properties of $(GeSe_2)_{100-x}(Sb_2Se_3)_x$ chalcogenide glasses as well as their structural properties are reported. Raman spectra are presented for various glassy compositions and reveal a progressive change when increasing Sb_2Se_3 content in the system, first favoring edge-shared [$GeSe_{4/2}$] edge linked entities. Sb_2Se_3 rich compositions appear to contain slightly higher number of Sb-Sb, Ge-Ge and Se-Se structural motifs.

Nonlinear properties of $(GeSe_2)_{100-x}(Sb_2Se_3)_x$ chalcogenide glasses are studied both at 1064 nm and at 1.55 µm. Evolution of n_2 and β are measured for different x values. Globally, nonlinear refractive index increases with increasing antimony content and figure of merit as high as 1.9-2.0 can be obtained at 1.55 µm. Furthermore, photosensitivity attributed to TPA is shown to be very dependent on composition. It is noteworthy that for glasses with intermediate Sb_2Se_3 content (at x = 30-40), photosensitivity is strongly reduced. At high power, a striking time varying transmission is also reported which is described with two dissimilar time constants. For instance, a fast photobleaching along with a slow photodarkening is observed in glasses with low Sb_2Se_3 content.

Acknowledgments

Czech Science Foundation (Project No. 13-05082S) and Ministry of Education, Youth, and Sports of the Czech Republic (Project CZ.1.07/2.3.00/30.0058 “Development of Research Teams at the University of Pardubice“) and the CNRS PICS (Projet International de Cooperation Scientifique) program financially supported this work. It was also realized in the framework of the French Labex “Action” and was partly supported by the RENATECH network and its FEMTO-ST technological facility. The authors thank prof. C. Focsa (Université de Lille) for Raman scattering spectra measurements.